Zhu et al. Journal of Orthopaedic Surgery and Research (2025) 20:202
https://doi.org/10.1186/s13018-025-05619-0

Journal of Orthopaedic Surgery and Research

RESEARCH

Open Access

Study on the mechanism of Shuanghe decoction against steroid-induced osteonecrosis of the femoral head: insights from network pharmacology, metabolomics, and gut microbiota

Kai Zhu[1†], Wanxin Liu[1†], Yuanyuan Peng[1†], Xiaoqiang Wang[1], Zhenhao Wang[1], Jun Zheng[1*], Guoying Deng[2*] and Qiugen Wang[1,2*]

Abstract

Background Steroid-induced osteonecrosis of the femoral head (SONFH) is a challenging and debilitating orthopedic condition with a rising incidence in recent years. Shuanghe Decoction (SHD), a traditional Chinese medicine formula, has shown significant efficacy in treating SONFH, though its underlying mechanisms remain unclear.

Purpose This study aims to elucidate the therapeutic effects and potential mechanisms of SHD on SONFH through in vivo experiments, combined with network pharmacology, metabolomics, and gut microbiota analysis.

Materials and methods Forty male Sprague-Dawley rats (300 ± 20 g) were randomly assigned to four groups: Control, Model, SHD-L, and SHD-H, with 10 rats each. SONFH was induced in all groups except the Control group using lipopolysaccharide and methylprednisolone. The SHD-L and SHD-H groups were treated with Shuanghe decoction at doses of 4.86 g/kg/day and 9.72 g/kg/day, respectively, for eight weeks. Bone morphology, pathological changes, and osteogenic factors were evaluated using Micro-CT, histological staining, and immunohistochemistry. Network pharmacology, metabolomics, and gut microbiota analyses were conducted to explore SHD's mechanisms.

Results SHD improved bone morphology and increased osteogenic factor expression (RUNX2, OCN, COL-I). Network pharmacology indicated that metabolic pathways play a key role in SHD's therapeutic effects. Metabolomic analysis

†Kai Zhu, Wanxin Liu and Yuanyuan Peng contributed equally to this work.

*Correspondence:
Jun Zheng
dudu8238@163.com
Guoying Deng
guoying.deng@shgh.cn
Qiugen Wang
wangqiugen@126.com

Full list of author information is available at the end of the article

identified 14 differential metabolites, including 21-hydroxypregnenolone and tyramine, which were restored to normal levels by SHD. Gut microbiota analysis revealed that SHD modulated bacterial abundance, particularly *Verrucomicrobia*, *Allobaculum*, and *Burkholderiales*. A comprehensive network identified two key metabolites (tyramine, 21-hydroxypregnenolone), seven targets (CYP19A1, CYP1A2, CYP1B1, CYP2C9, CYP3A4, MIF, and HSD11B1), two metabolic pathways (tyrosine metabolism, steroid hormone biosynthesis), and four bacterial taxa (*Jeotgalicoccus*, *Clostridium*, *Corynebacterium*, *rc4-4*) as central to SHD against SONFH.

Conclusion SHD alleviates SONFH by reshaping gut microbiota, reversing metabolic imbalances, and enhancing osteogenesis. Our findings provide novel insights into the pharmacological mechanisms of SHD, laying a foundation for its clinical application in treating SONFH.

Graphical Abstract

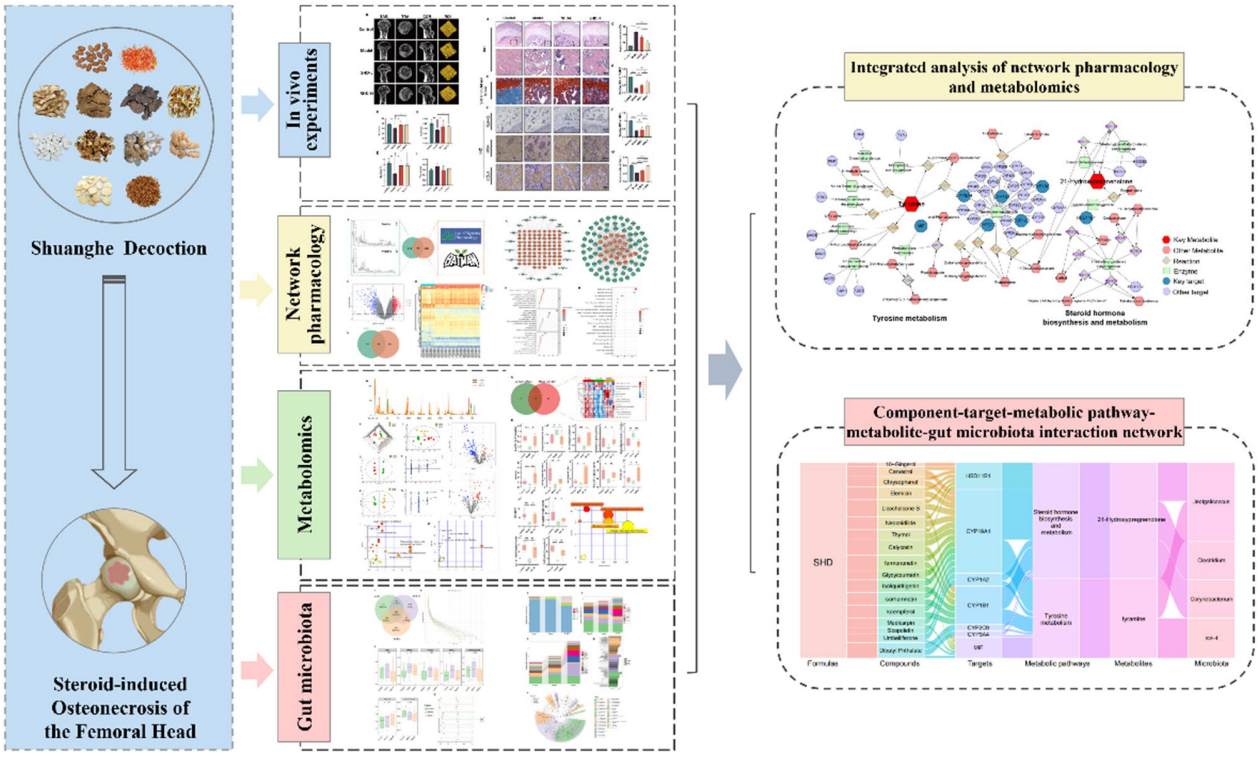

Keywords Shuanghe decoction, Steroid-induced osteonecrosis of the femoral head, Network pharmacology, Metabolomics, Gut microbiota

Introduction

Osteonecrosis of the femoral head (ONFH) is a globally refractory orthopedic condition characterized by the interruption of blood supply to the femoral head, leading to the necrosis of bone cells and bone marrow components [1]. Significant hip pain and functional impairment often result from structural changes and collapse of the femoral head, which can be caused by prolonged glucocorticoid use, excessive alcohol consumption, trauma, or other unidentified factors. With the increasing prevalence of long-term glucocorticoid use in the treatment of various immune disorders, the risk of steroid-induced osteonecrosis of the femoral head (SONFH) has also risen, making it the primary type of non-traumatic ONFH [2]. A recent study has noted a significant increase in SONFH cases, highlighting it as a major global public health concern [3].

The management of SONFH, particularly in the early stages, remains challenging due to the limited effectiveness of available treatments. Commonly used approaches such as core decompression (CD) and vascularized bone grafting (VBG) show promise but have limitations [4, 5]. CD, while frequently used, has been found to be ineffective in preventing the progression to total hip arthroplasty (THA) in the later stages [6]. A recent study indicates that the therapeutic benefits of CD are frequently compromised by incomplete restoration of vascular perfusion and procedural variability in drilling

dimensions and channel multiplicity [7]. Although bone marrow-derived cell therapies combined with CD have shown some improvement in clinical outcomes, this approach is still in its early stages and has not been widely adopted due to inconsistent results across studies [8]. Moreover, the availabid interventions like stem cell therapy and vascularized grafts raises additional concerns. While these therapies hold potential, their clinical application is hampered by issues such as high costs, technical challenges, and the variability of patient responses [5, 6]. Additionally, existing treatment protocolon, particularly regarding patient selection and the timing of interventions, making it difficult to compare the effectiveness of various strategies. Clinical data suggest that without effective intervention, 90% of ONFH patients will suffer femoral head collapse within five years, often necessitating THA [9]. However, THA is not ideal for younger patients due to the limited lifespan of prostheses and the high risk of complications from multiple revision surgeries [10, 11]. Thus, it is crucial to find effective treatments for early and mid-stage SONFH to delay femoral head collapse and postpone joint replacement surgeries.

Shuanghe Decoction (SHD) is a traditional Chinese medicine (TCM) formulation derived from the Qing Dynasty text *Za Bing Yuan Liu Xi Zhu* by Shen Jin'ao. It is composed of 12 Chinese herbs: *Persicae Semen* (Chinese: TaoRen), *Carthami Flos* (Chinese: HongHua), *Angelicae Sinensis Radix* (Chinese: DangGui), *Chuanxiong Rhizoma* (Chinese: ChuanXiong), *Radix Rehmanniae* (Chinese: ShengDiHuang), *Paeoniae Radix Alba* (Chinese: BaiShao), *Pinelliae Rhizoma* (Chinese: BanXia), *Citri Reticulatae Pericarpium* (Chinese: ChenPi), *Poria* (Chinese: FuLing), *Glycyrrhizae Radix Praeparata* (Chinese: GanCao), *Sinapis Albae Semen* (Chinese: BaiJieZi), and *Zingiberis Rhizoma Recens* (Chinese: ShengJiang). From the perspective of TCM, SHD is a modified formula derived from Taohong Siwu Decoction and Erchen Decoction, known for its ability to invigorate blood circulation, remove blood stasis, resolve phlegm, and unblock the meridians. Modern pharmacological studies have revealed that Erchen Decoction can regulate lipid metabolism, reduce blood viscosity, and enhance local blood supply [12]. Similarly, Taohong Siwu Decoction has been found to promote blood circulation, improve local blood supply, and facilitate osteogenic differentiation [13]. Clinically, Taohong Siwu Decoction is commonly used in the treatment of fractures or ONFH [14]. Furthermore, SHD is widely used in clinical practice, both as a monotherapy and in combination with surgical interventions, for various types of non-traumatic ONFH, consistently demonstrating significant efficacy. Previous studies have shown that Shuanghe Decoction can promote the repair of necrotic bone, increase bone density, improve lipid metabolism disorders, and effectively delay the progression of NONFH [15, 16]. Despite these promising findings, the precise mechanisms underlying the therapeutic effects of SHD on SONFH remain unclear, which hinders its broader clinical application. Therefore, further investigation into the molecular mechanisms of SHD is imperative.

TCM and its formulations offer advantages such as multi-component and multi-target actions, broad biological activities, and favorable efficacy and safety profiles. However, the complexity of active components and the unclear mechanisms of action in TCM treatments have limited their development [17]. Scientific analysis to elucidate the potential mechanisms of TCM is crucial for advancing drug development and utilization. At present, multi-omics and multi-dimensional analyses are becoming essential in TCM research, enhancing our understanding of disease progression and treatment mechanisms. Network pharmacology, combined with phenotypic screening, can identify therapeutically valuable compounds, facilitating systematic research on bioactive components [18]. Furthermore, gut microbiota, central to TCM research, plays a crucial role in host health, and its interactions with TCM can be analyzed using 16S rRNA sequencing. Additionally, metabolomics, an advanced systems biology technique, tracks dynamic changes in metabolites and characterizes systemic metabolic responses of complex diseases [19]. Its holistic nature aligns well with approach of TCM, showing great potential in evaluating TCM bioactivity and studying mechanisms of action.

This study investigated the pharmacodynamic effects of SHD on SONFH through in vivo experiments. By integrating network pharmacology, metabolomics, and gut microbiota analysis, we systematically elucidated the metabolic and gut microbial profiles associated with SHD treatment in SONFH rats. These comprehensive analyses shed light on the potential mechanisms underlying therapeutic effects of SHD on SONFH. Overall, our research enhances understanding of the pharmacodynamic mechanisms of SHD, providing a basis for its clinical application and promoting its development and utilization.

Materials and methods

Preparation of Shuanghe Decoction

All herbs in SHD were provided by the Yueyang Hospital of Integrated Traditional Chinese and Western Medicine, Shanghai University of Traditional Chinese Medicine, and identified by two experienced traditional Chinese medicine practitioners. Detailed information about the herbs in SHD is shown in TableS1. The herbs were soaked in eight times their volume of distilled water for 30 min, then boiled for 30 min. The liquid was filtered, and another six times the volume of distilled water was added to the residue, followed by another 30-minute

boil. The second liquid was filtered and combined with the first filtrate. The combined filtrate was concentrated under reduced pressure (-0.04 to 0.01 MPa, 60 °C) to a relative density of 1.05, and the supernatant was collected by centrifugation at 6,000 rpm, then stored at 4 °C.

Model construction, grouping, and intervention of experimental animals

Forty male Sprague-Dawley (SD) rats, weighing 300 ± 20 g, were provided by Shanghai Jihui Laboratory Animal Breeding Co., Ltd. (Shanghai, China, production license number: SCXK 2022-0009). The animals were acclimated for one week under standard laboratory conditions (temperature 22–26℃, relative humidity 50–60%, 12-hour light/dark cycle). This study was approved by the Animal Ethics Committee of Yueyang Hospital of Integrated Traditional Chinese and Western Medicine, Shanghai University of Traditional Chinese Medicine (approval ID: YYLAC-2023-184). The SD rats were randomly divided into four groups using a random number table method: Control group ($n = 10$); Model group ($n = 10$); low-dose Shuanghe Decoction group (SHD-L, $n = 10$); high-dose Shuanghe Decoction group (SHD-H, $n = 10$). A rat model of SONFH was established using methylprednisolone (MPS) combined with lipopolysaccharide (LPS). Except for the control group, the other three groups received intraperitoneal injections of LPS (20 μg/kg, Sigma-Aldrich, USA) once daily for three consecutive days, with a 24-hour interval between each injection. This was followed by intramuscular injections of MPS (40 mg/kg, Pfizer, USA) once daily for four consecutive days and once a week for the next three weeks [20]. Four weeks later, two rats were randomly selected from each group, and their femoral heads were harvested for hematoxylin and eosin (HE) staining to histologically evaluate the successful establishment of SONFH. The SHD-L group and SHD-H group were administered Shuanghe Decoction by gavage at doses of 4.86 g/kg/day and 9.72 g/kg/day, respectively. The control and model groups were administered physiological saline by gavage. All interventions were conducted once daily for eight consecutive weeks.

Sample collection

After eight weeks of intervention, all rats were euthanized. Under sterile conditions, the abdominal cavity was opened, exposing the rectum and cecum. Using sterile surgical scissors, the rectum was carefully opened, and feces were squeezed into a sterile centrifuge tube, avoiding contact with other contaminants. Similarly, sterile surgical scissors were used to open the cecum, and the contents were gently squeezed into a sterile centrifuge tube, with visible impurities removed. After weighing, the fecal and cecal contents were aliquoted and immediately frozen in liquid nitrogen before being transferred to -80 °C for long-term storage. Fecal samples were used for metabolomics analysis, while cecal contents were used for 16S rRNA sequencing. Finally, the femoral heads were collected into centrifuge tubes, fixed with 4% paraformaldehyde solution, and prepared for micro-computed tomography (Micro-CT) and subsequent staining analysis.

Micro-CT scanning analysis

Fixed femoral head samples from all four groups were scanned using a Siemens Inveon micro-CT scanner (Siemens, Germany) with a resolution of 9 μm to evaluate trabecular bone morphology. Inveon Acquisition Workplace software (Siemens, Germany) was employed to reconstruct images of the sagittal, coronal, and transverse planes of the femoral head. A cubic region of interest (ROI) measuring 2 × 2 × 1 mm was selected in the subchondral bone of the femoral head for analysis. The following parameters were calculated: bone volume fraction (BV/TV), trabecular thickness (Tb.Th), trabecular number (Tb.N), and trabecular separation (Tb.Sp).

Hematoxylin-Eosin (HE) and Safranin-O-Fast green staining

After fixation, the femoral head tissues were decalcified using 10% ethylene diamine tetraacetic acid (EDTA) for six weeks. Once decalcified, the samples were embedded in paraffin, sectioned with a microtome, and mounted onto glass slides. The sections were then dehydrated with xylene and a graded series of alcohol. Subsequently, they were stained with hematoxylin and eosin, and also with Safranin O/Fast Green. Finally, the stained sections were photographed using a microscope (Olympus Corporation, Japan). The percentage of empty lacunae within the sections was quantitatively evaluated [21].

Immunohistochemistry(IHC) staining

IHC was used to detect the expression of RUNX2, OCN, and COL-I. Briefly, the tissue sections were deparaffinized and quenched with 3% hydrogen peroxide for 10 min, followed by blocking with 10% normal goat serum. The sections were then incubated overnight at 4℃ with rabbit anti-rat RUNX2, OCN, and COL-I antibodies (1:200, Abcam, UK). Afterward, the sections were incubated with horseradish peroxidase (HRP)-conjugated goat anti-rabbit IgG. Finally, the sections were treated with DAB and counterstained with hematoxylin. Quantitative analysis of the positive staining images was performed using Image-Pro Plus 6.0 software.

Identification of active components in SHD by ultra-high performance liquid chromatography-quadrupole exactive orbitrap mass spectrometry (UHPLC-Q Exactive Orbitrap MS)

A 1 mL aliquot of the prepared SHD (1 g/mL) was dissolved in 10 mL of ultrapure water and vortexed for 1 min. The mixture was then subjected to ultrasound in an ice bath for 10 min. The sample was treated with methanol at three times its volume, vortexed for 1 min, and centrifuged at 13,000 rpm for 15 min. The supernatant was collected and analyzed using a Q Exactive-Orbitrap MS system (Thermo Fisher Scientific, USA).

Chromatographic conditions for the C18 column were as follows: the column used was an ACQUITY UPLC BEH C18 (100 mm × 2.1 mm i.d., 1.7 μm; Waters, Milford, USA). The mobile phase consisted of solvent A (2% acetonitrile in water containing 0.1% formic acid) and solvent B (acetonitrile containing 0.1% formic acid). The injection volume was 3 μL, and the column temperature was maintained at 40 °C.

Mass spectrometry conditions included electrospray ionization (ESI) with both positive and negative ion scan modes used to acquire the mass spectra. The data obtained were processed using Progenesis QI v3.0 (Waters Corporation, USA) for peak extraction, alignment, and identification. The final data matrix included retention time, peak area, mass-to-charge ratio, and identification information.

Network pharmacology and bioinformatics analysis

Active components of each herb in Shuanghe Decoction were predicted using the TCMSP (https://www.tcmsp-e.com/) database with criteria set to oral bioavailability (OB) ≥ 30% and drug-likeness (DL) ≥ 0.18, and the BATMAN (http://bionet.ncpsb.org.cn/batman-tcm/) database with target prediction score set to 20 and target analysis P-value set to 0.05. The predicted components were then intersected with those identified by UHPLC-Q Exactive Orbitrap MS. SMILES codes for the intersected components were retrieved from the PubChem database and entered into the Swiss Target Prediction database with an inclusion criterion of Probability > 0 for target retrieval. Duplicates were removed from the consolidated target list.

mRNA microarray data related to SONFH were downloaded from the GEO database, specifically the raw microarray data for GSE123568 and the microarray gene annotation file for GPL15207. The raw data included 40 serum samples, with 30 from SONFH patients and 10 from healthy controls. The raw microarray files were re-analyzed using R software (version 4.2.1), with significant differential genes identified using a threshold of $P < 0.05$ and Fold Change (FC) > 2. Additionally, SONFH disease targets were identified using keywords "steroid-induced osteonecrosis of the femoral head" in databases such as OMIM (http://www.omim.org/), GeneCards (https://www.genecards.org/), and KEGG (https://www.kegg.jp/), combined with results from the Uniprot database and GEO analysis, with duplicates removed to finalize the list of SONFH disease targets.

A Venn diagram was utilized to visualize the intersection of drug and disease targets, and a compound-target network was constructed. The intersected targets identified from the Venn diagram were imported into the STRING database for protein-protein interaction (PPI) analysis. Core PPI targets were analyzed using Cytoscape 3.9.0. GO and KEGG analyses of related target genes were conducted using the DAVID database (https://david.ncifcrf.gov/), and relevant bubble charts were generated for visualization.

Metabolomics analysis

Fecal samples were thawed on ice, from which 50 mg was taken and mixed with ultra-pure water and the internal standard 4-chlorophenylalanine (1 mg/mL), followed by grinding. A 300 μL mixture of methanol and chloroform (3:1, v/v) is added and homogenized twice, then the mixture is allowed to stand at -20 °C for 20 min. After centrifugation at 12,000 rpm and 4 °C for 20 min, the supernatant was transferred to an autosampler vial and lyophilized. The lyophilized sample was derivatized first with a pyridine solution containing hydrochloric acid methoxyamine, and subsequently with MSTFA (1% TMCS) for secondary derivatization. The analysis was performed using an Agilent 7890B gas chromatography system coupled with a Leco Pegasus time-of-flight mass spectrometer (Leco Corporation, St. Joseph, MI, USA).

Chromatographic separation was achieved using a Restek RXi-5ms capillary column (30 m × 0.25 mm i.d., 0.25 μm film thickness), coated with 5% diphenyl cross-linked with 95% dimethylpolysiloxane (Restek Corporation, Bellefonte, PA, USA). Helium was used as the carrier gas at a constant flow rate of 1.0 mL/min. The temperature program started at 80 °C for 2 min, then increased at a rate of 12 °C per minute to 300 °C, and held for 5.7 min. The total run time was 26 min, with a solvent delay of 4.6 min. The injection, transfer line, and ion source temperatures were set at 270 °C, 270 °C, and 220 °C, respectively. Electron impact ionization was performed at -70 eV, with a data acquisition rate of 20 spectra per second.

16S rRNA analysis

The 16S rRNA analysis of cecal contents from each group was performed by Metabo-Profile Biotechnology Co., Ltd. (Shanghai, China). Firstly, the microorganisms were isolated and purified, and total DNA was extracted. Next, the bacterial 16S rRNA gene (V3-V4

region) was amplified in triplicate using specific primers: 338F (5'-ACTCCTACGGGAGGCAGC3') and 806R (5'-GGACTACHVGGGTWTCTAAT-3'). Subsequently, the PCR products were extracted from 2% agarose gels and purified using the AxyPrep DNA Gel Extraction Kit (Axygen Biosciences, Union City, CA, USA). Finally, the purified amplification products were mixed in equimolar amounts and sequenced on the Illumina MiSeq PE300 platform (Illumina, San Diego, CA, USA). The results were analyzed based on sequencing reads and operational taxonomic units (OTUs).

Construction of the compound-target-metabolic pathway-metabolite-gut microbiota network

In this study, we initially performed a Spearman correlation analysis on differential genera and metabolites based on available microbiome and metabolomics datasets. Correlation heatmaps were subsequently generated using R to visualize these associations. Following this, we imported the differential metabolites identified through the metabolomics analysis and the intersecting targets determined via network pharmacology into the MetScape plugin in Cytoscape. This process enabled the identification of key targets, significant metabolites, and core metabolic pathways, which were depicted in a "metabolite-reaction-enzyme-target" network. Ultimately, we integrated these findings to construct a comprehensive compound-target-metabolic pathway-metabolite-gut microbiota network. This network was illustrated by a Sankey diagram to effectively depict the complex interactions and intricate relationships among these components.

Statistical analysis

All statistical analyses were conducted using GraphPad Prism 9.5 (GraphPad Software, San Diego, CA, USA) and R statistical environment (version 4.2.1; R Foundation for Statistical Computing, Vienna, Austria). Continuous variables were characterized by their distributional properties: normally distributed parameters are presented as mean ± standard deviation (SD), analyzed using parametric methods including Student's t-test for dual-group comparisons or one-way ANOVA with Tukey's honestly significant difference (HSD) post hoc test for multi-group analyses. Non-normally distributed continuous variables were expressed as median with interquartile range (IQR) [25th-75th percentiles], with between-group differences assessed via Mann-Whitney U test. The correlation between two variables was analyzed using Pearson's correlation analysis. Categorical variables were summarized using frequency distributions with proportional percentages. Intergroup comparisons for nominal data employed Pearson's χ^2

Results

SHD enhances osteogenic capability against SONFH in vivo

To evaluate the therapeutic effects of SHD on SONFH in rats, we employed Micro-CT, HE staining, and Safranin-O-Fast Green staining for morphological assessment. Micro-CT imaging and morphological parameters revealed that, compared to the control group, the model group exhibited sparse trabeculae and significant bone loss in the femoral head, indicated by irregular low-density areas (Fig. 1A). Additionally, the model group showed decreases in BV/TV, Tb.Th, and Tb.N, with no significant change in Tb.Sp (Fig. 1B-E). In contrast, both the SHD-L and SHD-H groups demonstrated improved femoral head morphology, with increases in BV/TV, Tb.Th, and Tb.N, while Tb.Sp remained unchanged (Fig. 1A-E).

Histological analysis using HE (Fig. 2A) and Safranin-O-Fast Green staining (Fig. 2B) indicated no noticeable necrosis in the control group. In the model group, however, the femoral head exhibited sparse trabeculae, an increase in adipocytes, a high rate of empty lacunae (Fig. 2C), and marked necrosis. The SHD-L and SHD-H groups showed significant improvements in these parameters compared to the model group, with a lower rate of empty lacunae, and the SHD-H group showing better outcomes than the SHD-L group. These histological findings were consistent with the Micro-CT results, suggesting that SHD provides protection against trabecular bone loss induced by LPS and MPS.

Immunohistochemical analysis (Fig. 2D-G) further demonstrated that the expression levels of osteogenic markers RUNX2, OCN, and COL-I were significantly lower in the model group compared to the control group. Treatment with the high-dose SHD reversed these changes, restoring the expression levels of these markers. Notably, the low-dose SHD also increased COL-I expression compared to the model group, but did not significantly affect RUNX2 and OCN levels ($P > 0.05$).

Network pharmacology investigates the mechanisms of SHD in treating SONFH

In this study, a total of 307 active components of SHD were identified from the TCMSP and BATMAN databases. Additionally, analysis of UHPLC-Q Exactive Orbitrap MS results revealed 396 active components. By intersecting these datasets, 25 core components were identified (Fig. 3A and Table S2). Through the PubChem and Swiss Target Prediction databases, 523 candidate targets for these core components were predicted. Furthermore, secondary analysis of gene expression data from the GEO chip database, performed with the illumina

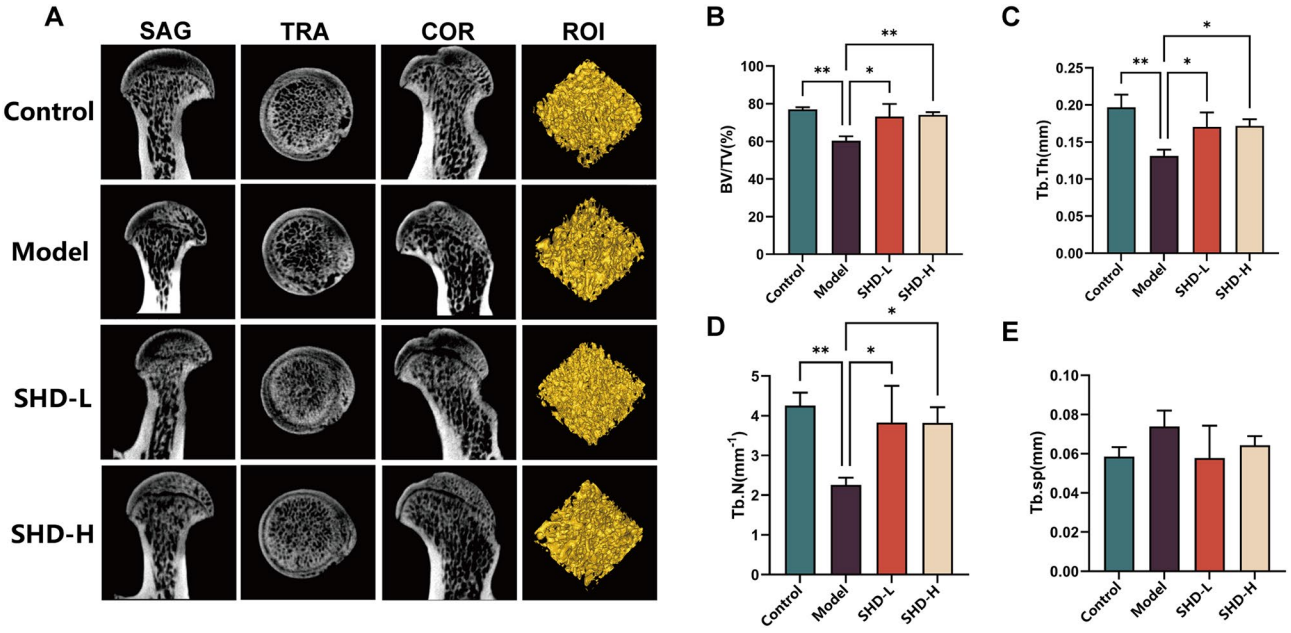

Fig. 1 SHD inhibited bone loss of the femoral head in rats with SONFH. Micro-CT Analysis of Trabecular Bone Microarchitecture in Different Experimental Groups. (**A**) Representative micro-CT images of the trabecular bone in sagittal (SAG), transverse (TRA), coronal (COR) planes, and three-dimensional reconstructed images of the region of interest (ROI) from different groups: Control, Model, SHD-L, and SHD-H. Quantitative analysis of BV/TV (**B**), Tb.Th (**C**), Tb.N (**D**), Tb.Sp (**E**). Data are presented as mean ± SD, $n = 3$. $^{**}P < 0.01$, $^{*}P < 0.05$. Abbreviations: SHD, Shuanghe Decoction; BV/TV, bone volume/tissue volume; Tb.Th, trabecular thickness; Tb.N, trabecular number; Tb.Sp, trabecular separation

package in R, identified 594 differentially expressed genes potentially associated with the development of SONFH (Fig. 3B-C). Additional targets were collected from the OMIM, GeneCards, and KEGG databases, resulting in a total of 341 SONFH-related targets. After removing duplicates, 903 candidate gene targets were included. Cross-analysis of the 523 drug targets and 903 disease targets revealed 93 shared targets (Fig. 3D and Table S3).

The core components of SHD and the 93 shared drug-disease targets were imported into Cytoscape 3.9.0 to construct a compound-target network, where green nodes represent SHD active components and red nodes represent shared targets (Fig. 4A). To further explore the mechanisms of these potential targets, the 93 intersecting targets were uploaded to the STRING 12.0 database for network topology analysis, with protein type set to "Homo sapiens" and the minimum interaction threshold set to 0.4. The STRING results were then imported into Cytoscape 3.9.0, and isolated nodes were removed to construct the protein-protein interaction (PPI) network. This network consisted of 93 nodes and 1,107 edges, with an average node degree of 23.8. Red circles indicated core targets with a degree value greater than 30 (Fig. 4B). GO and KEGG analyses of the 93 common targets were conducted through the DAVID database. The GO analysis results showed that these common targets were enriched in 429 biological process pathways, 53 cellular component expression processes, and 120 molecular function-related processes. The top 10 results from each category were visualized in a bubble chart (Fig. 4C and Table S2). Additionally, KEGG pathway analysis revealed significant enrichment in 126 pathways, with the top 20 entries shown in Fig. 4D and Table S5. Notably, Metabolic pathways demonstrated significant relevance in the therapeutic intervention of SONFH with SHD.

SHD reverses metabolic disorders in SONFH rats

Our preliminary network pharmacology analysis suggested that the therapeutic mechanism of SHD in treating SONFH is closely related to Metabolic pathways. To further elucidate these metabolic changes, we conducted a fecal metabolomics study on the Control, Model, and SHD-H groups using GC-TOF/MS. The total ion chromatograms (TIC) for the three groups are presented in Fig. 5A, identifying 642 relevant metabolites in rat fecal samples.

We then performed an unsupervised PCA analysis of the metabolomics data, as shown in Fig. 5B-C. The Control, Model, and SHD-H groups displayed distinct intra-group clustering and inter-group separation, with a model explanation rate (R2X) of 0.369 and a model prediction rate (Q2) of 0.112. The SHD-H group positioned between the Control and Model groups, indicating a clear trend towards the Control group.

Next, a supervised OPLS-DA model was used to examine the differences between the Control and Model groups, and between the SHD-H and Model groups. Figure 5D-G demonstrate that both the Control and SHD-H

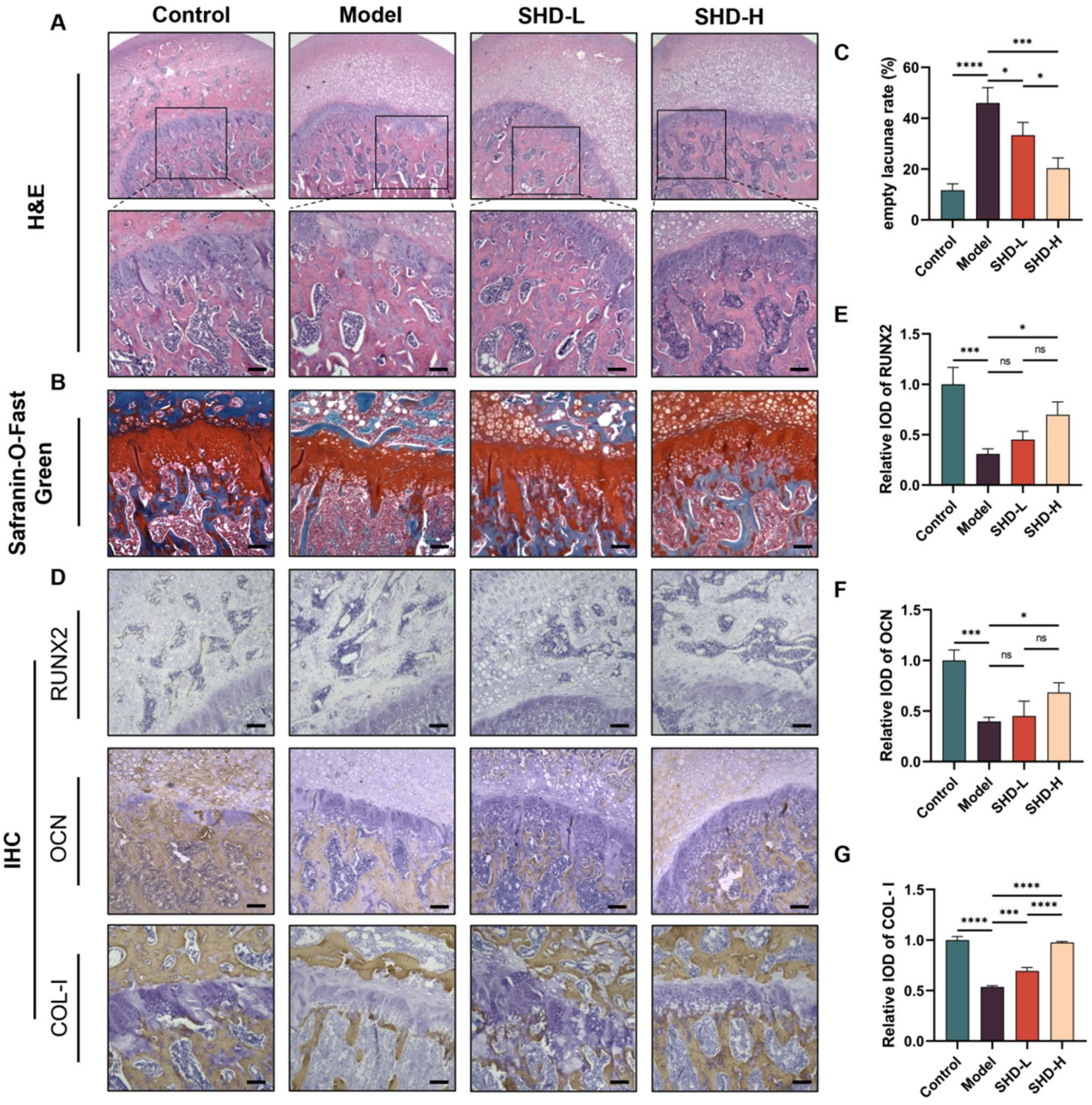

Fig. 2 SHD alleviated the progression of femoral-head necrosis in vivo. (**A**) Representative images of HE staining in the femoral head from Control, Model, SHD-L, and SHD-H groups. The upper panels show low magnification, and the lower panels show high magnification of the boxed areas. (**B**) Safranin-O-Fast Green staining of the femoral head from different groups. (**C**) Statistical analysis of empty lacunae rate. (**D**) Representative images of RUNX2, OCN, and COL-I by immunohistochemical assay. (**E**) Quantification of the relative integrated optical density (IOD) of RUNX2. (**F**) Quantification of the relative IOD of OCN. (**G**) Quantification of the relative IOD of COL-I. Data are presented as mean ± SD, $n = 3$. ****$P < 0.0001$, ***$P < 0.001$, **$P < 0.01$, *$P < 0.05$, ns $P > 0.05$. Scale bars: 100 μm. Abbreviations: SHD, Shuanghe Decoction; HE, hematoxylin and eosin; IHC, immunohistochemistry

groups were distinctly separated from the Model group. The model parameters for the Control versus Model comparison were R2X = 0.557, R2Y = 0.995, and Q2 = 0.725; for the SHD-H versus Model comparison, the parameters were R2X = 0.275, R2Y = 0.978, and Q2 = 0.531.

To further analyze the metabolites, We filtered the 642 identified metabolites with criteria: Student' s t-test p-value < 0.05, OPLS-DA VIP > 1, and 1.2 < FC < 0.8, identifying 101 differential metabolites between the Control and Model groups (Fig. 5H) and 44 between the SHD-H and Model groups (Fig. 5I). Metabolic pathway analysis of these metabolites was performed with MetaboAnalyst. As shown in Figs. 5J and 11 significant metabolic pathways (impact > 0.1) were disturbed in the Control group

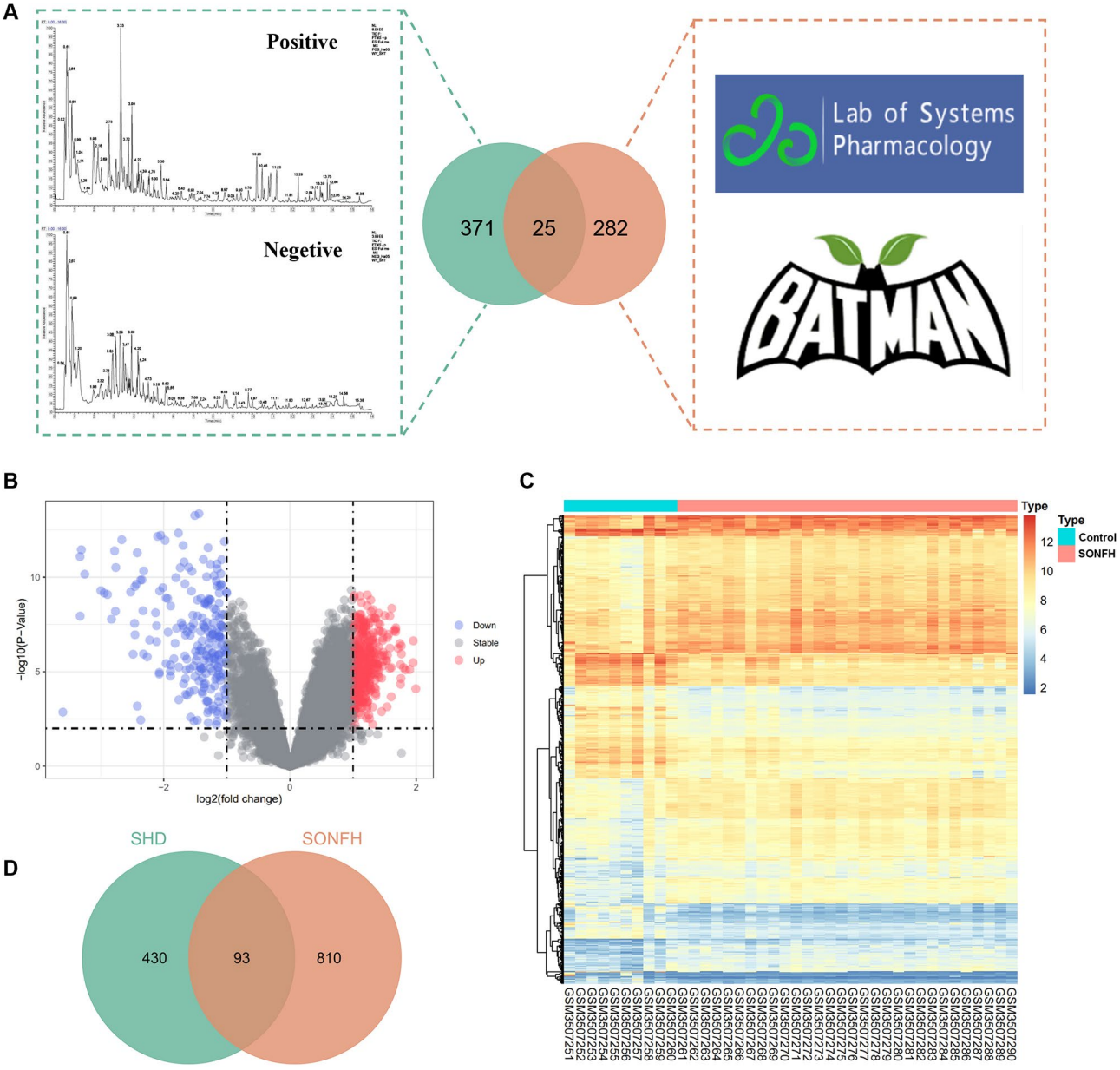

Fig. 3 Target identification and mapping Analysis of SHD and SONFH. (**A**) 396 compounds from SHD were identified by UHPLC-Q Exactive Orbitrap MS; 307 compounds contained in SHD were collected from databases; 25 compounds were finally screened as the putative and representative compounds of SHD. Volcanogram (**B**) and cluster diagram (**C**) of SONFH differentially expressed genes from GSE123568 data in GEO database. (**D**) Venn diagram showing the intersection of drug targets of SHD and disease targets of SONFH

compared to the Model group, including starch and sucrose metabolism, TCA cycle, tyrosine metabolism, arginine biosynthesis, glycerophospholipid metabolism, phenylalanine, tyrosine, and tryptophan biosynthesis, D-glutamine and D-glutamate metabolism, alanine, aspartate and glutamate metabolism, phenylalanine metabolism, pentose phosphate pathway, and lysine degradation. Analysis of the differential metabolites between the SHD-H and Model groups suggested that SHD may exert its therapeutic effects on SONFH through four key metabolic pathways (impact > 0.1): pyruvate metabolism, linoleic acid metabolism, glycolysis/gluconeogenesis, and inositol phosphate metabolism (Fig. 5K).

Additionally, the Venn diagram (Fig. 6A) illustrates the relationships among the differential metabolites identified in each group. We identified 14 common metabolites, namely: 2-methyl-6-ethylpyrazine, 6-hydroxyhexanoic acid, O-phosphorylethanolamine, Methyl-beta-D-galactopyranoside, N(alpha), N(alpha)-dimethyl-L-histidine, tyramine, methyl hexadecanoate, coniferyl alcohol, N-acetyl-D-galactosamine, ferulic acid, naringenin, 21-hydroxypregnenolone,

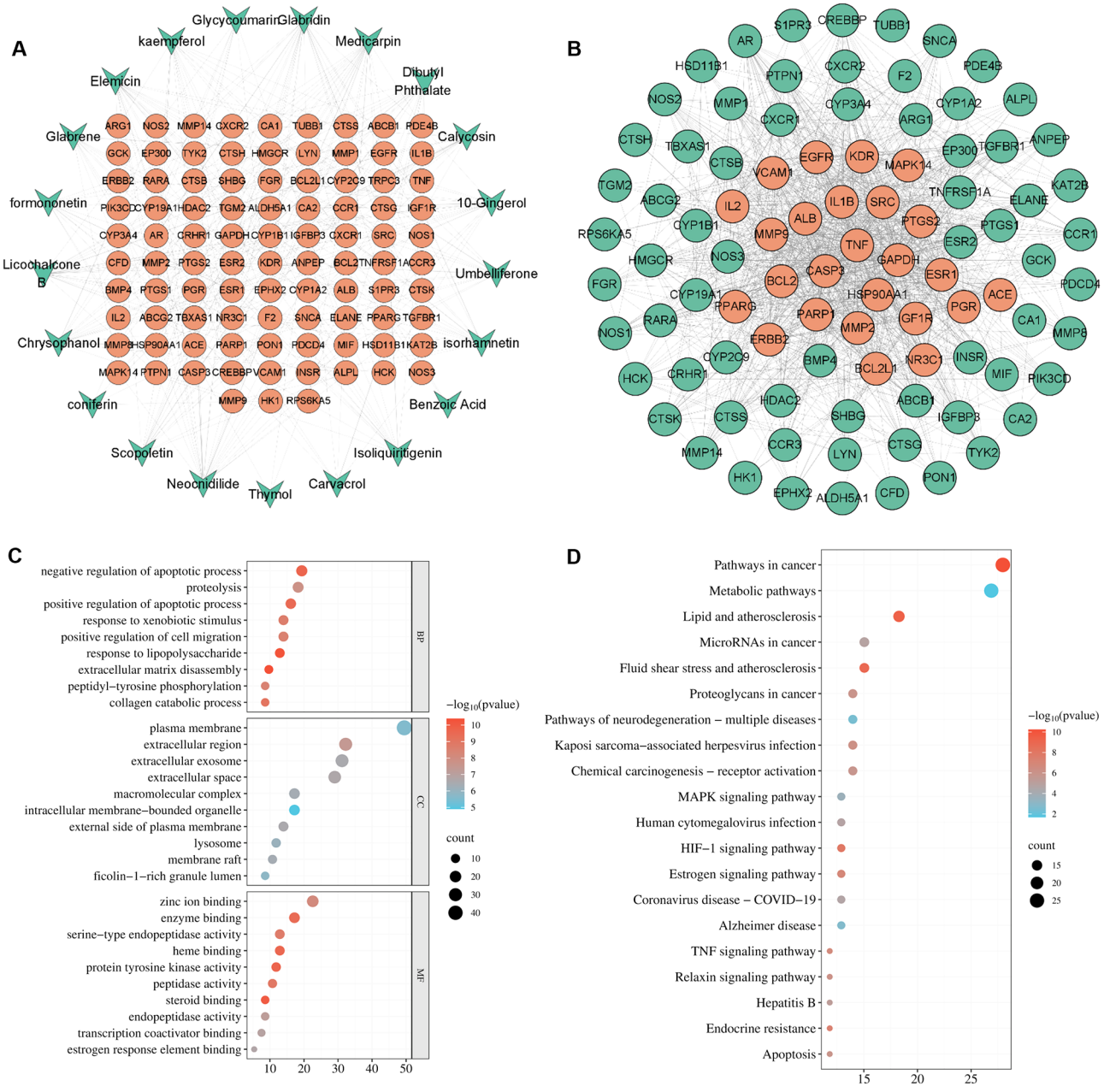

Fig. 4 Network pharmacology and functional enrichment analysis of SHD against SONFH. (**A**) Compound-target network of SHD. The network illustrates the interaction between bioactive compounds of SHD (green diamonds) and SHD-SONFH targets (orange circles). (**B**) Protein-protein interaction (PPI) network of SONFH targets. Green circles represent identified targets, and orange circles represent core targets (degree-value > 30). (**C**) Gene Ontology (GO) enrichment analysis of the identified targets, categorized into biological processes (BP), cellular components (CC), and molecular functions (MF). In bubble chart, the x-axis represents the number of genes involved, and the color gradient indicates the -log10 (P-value) of the enrichment significance. (**D**) Kyoto Encyclopedia of Genes and Genomes (KEGG) pathway enrichment analysis of the identified targets, and the top 20 significant terms were visualized by bubble chart. The x-axis represents the number of genes involved in each pathway, and the color gradient indicates the -log10 (P-value) of the enrichment significance

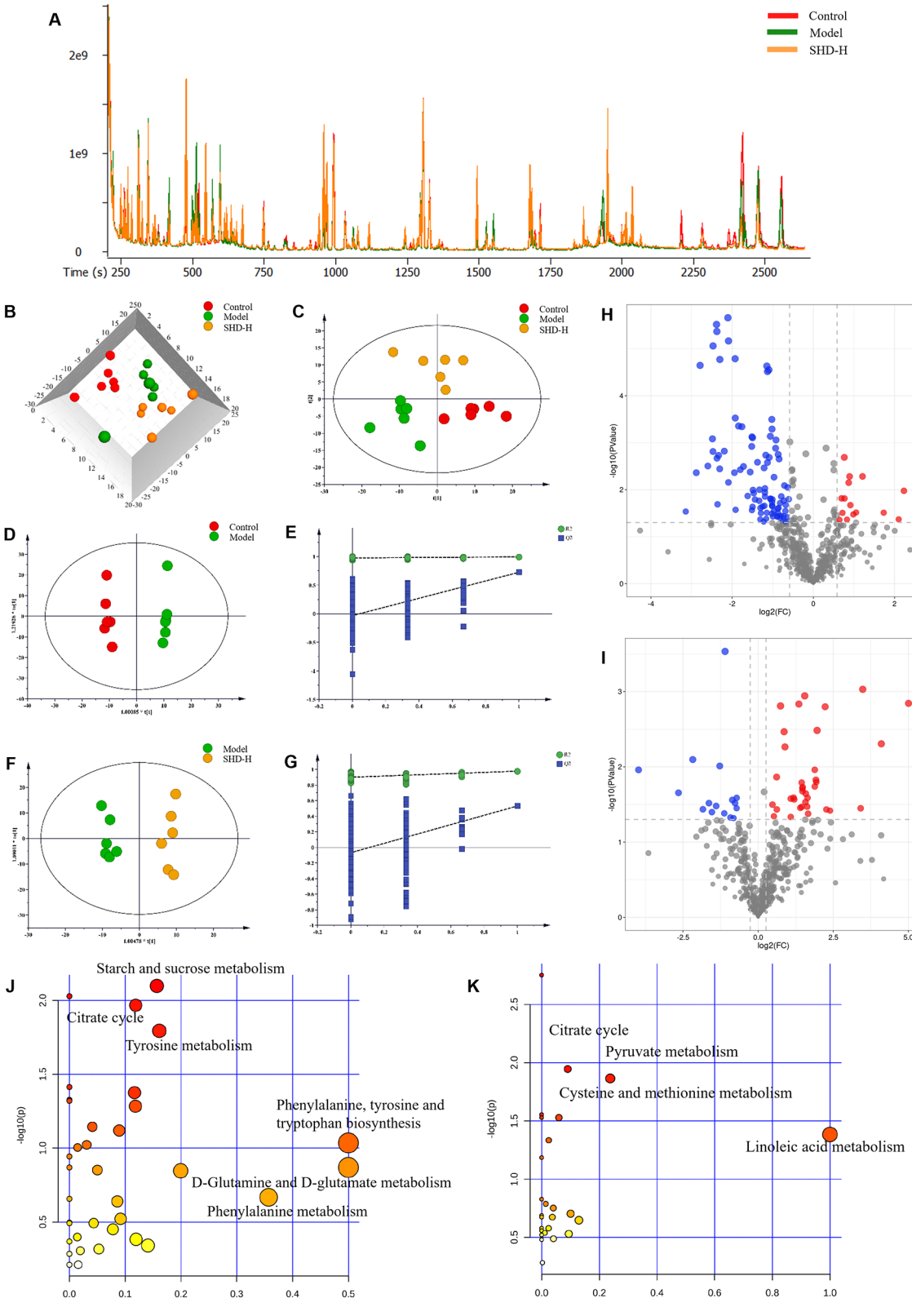

Fig. 5 (See legend on next page.)

(See figure on previous page.)

Fig. 5 Multivariate statistical analysis of metabolomics. (**A**) TIC of fecal samples from Control, Model, and SHD-H groups. (**B**) Three-dimensional PCA score plot showing the separation of metabolic profiles among Control, Model, and SHD-H groups. Each point represents an individual sample, demonstrating the clustering and separation of metabolic signatures. (**C**) Two-dimensional PCA score plot of the Control, Model, and SHD-H groups, illustrating the clustering of samples based on their metabolic profiles, and indicating distinct metabolic shifts among the groups. OPLS-DA (Orthogonal Partial Least Squares Discriminant Analysis) score plot comparing the Control group and the Model group (**D**), as well as the Model and SHD-H groups (**F**). Permutation test results of the OPLS-DA model for the Control and Model groups (**E**), as well as the Model and SHD-H groups (**G**). Volcano plot of differentially expressed metabolites between groups: Control vs. Model groups (**H**), Model vs. SHD-H groups (**I**). Metabolic pathway analysis of differentially expressed metabolites between groups: Control vs. Model groups(**J**), Model vs. SHD-H groups (**K**). Abbreviations: TIC, total ion chromatograms; PCA, principal component analysis; OPLS-DA, orthogonal partial least squares discriminant analysis

3,7,12-Trihydroxycoprostane, and 24,25-dihydrolanosterol. The expression levels of these metabolites in different groups are shown in Fig. 6B. These metabolites were altered following the establishment of the SONFH model and were reversed upon SHD treatment. Metabolic pathway analysis of the 14 differential metabolites using MetaboAnalyst indicated significant enrichment in sphingolipid metabolism, glycerophospholipid metabolism, tyrosine metabolism, and primary bile acid biosynthesis (Fig. 6C).

SHD alters gut microbiota composition in SONFH rats

We found that SHD impacts the fecal metabolites of SONFH rats, which are often closely related to gut microbiota. Therefore, we conducted 16S rRNA sequencing on fecal samples from the Control, Model, and SHD-H groups. First, we clustered ASVs with similarity levels > 95% into OTUs, considering each OTU as a single species. The Venn diagram (Fig. 7A) shows 2,930 ASV/OTUs identified, with 314 common among all groups. The Control, Model, and SHD-H groups had 659, 742, and 879 unique ASV/OTUs, respectively. Species abundance and evenness, important indicators of gut microbiota composition, are depicted in Fig. 7B. Alpha diversity, shown in Fig. 7C, measures within-sample microbial diversity, reflecting richness and evenness of the microbial community. We used unweighted pair group method with arithmetic mean (UPGMA) clustering to represent the similarity between samples. The UPGMA dendrogram (Fig. 7D) indicates clear separation among the Control, Model, and SHD-H groups.

Next, we evaluated the species-related abundance at different taxonomic levels to assess gut microbiota composition across groups. Figure 8A-C show the major bacterial communities at the phylum, family, and genus levels. At the phylum level (Fig. 8A), 13 phyla were identified, primarily consisting of *Firmicutes*, *Actinobacteria*, *Bacteroidetes*, and *Proteobacteria*. At the family level (Fig. 8B), the major families included *Lactobacillaceae*, *S24-7*, *Desulfovibrionaceae*, *Ruminococcaceae*, *Lachnospiraceae*, *Coriobacteriaceae*, and *Erysipelotrichaceae*. Genus-level analysis (Fig. 8C) revealed that SHD-H increased the relative abundance of *Dorea* and *Enterococcus* and decreased *Ruminococcus* and *Allobaculum* compared to the Model group. Additionally, beneficial *Akkermansia* increased significantly in the SHD-H group.

Lastly, we performed LEfSe differential analysis, identifying significant differences in bacterial species across groups using LDA scores. Species with an LDA > 3.0 were considered statistically significant biomarkers. Combining with phylogenetic branch analysis, we identified 44 bacterial taxa with varying abundance levels among groups (Fig. 8D, E). In the Control group, the most significant species were *Christensenella*, *Adlercreutzia*, *Ruminococcus*, *Mollicutes*, and *Clostridia*. In the Model group, species such as *Aerococcaceae*, *Ruminococcaceae*, *Corynebacteriaceae*, *Desulfovibrionales*, and *Facklamia* were notably affected, suggesting their association with SONFH. SHD led to significant changes in *Verrucomicrobia*, *Allobaculum*, *Verrucomicrobiaceae*, *Erysipelotrichales*, and *Burkholderiales*. These findings indicate that SHD modulates gut microbiota composition in SONFH rats, and these microbial changes could serve as biomarkers for SHD treatment efficacy and gut health improvement in SONFH.

Integrative analysis based on gut microbiome, metabolomics, and network pharmacology

In this study, a Spearman correlation analysis was performed on different genera of gut microbiota and differential metabolites based on available microbiome and metabolomics data. The analysis revealed correlations between 14 differential metabolites and 15 bacterial genera, as detailed in the correlation heatmap (Fig. 9A). Subsequently, intersecting targets from network pharmacology were matched with differential metabolites from metabolomics via Metscape, resulting in the identification of 2 key metabolites (tyramine, 21-hydroxypregnenolone), 7 targets (CYP19A1, CYP1A2, CYP1B1, CYP2C9, CYP3A4, MIF, HSD11B1), and 2 metabolic pathways (tyrosine metabolism, steroid hormone biosynthesis and metabolism), presented in a "metabolite-reaction-enzyme-target" network (Fig. 9B). Finally, based on these results, a comprehensive "compound-target-metabolic pathway-metabolite-gut microbiota" interaction network was constructed (Fig. 9C).

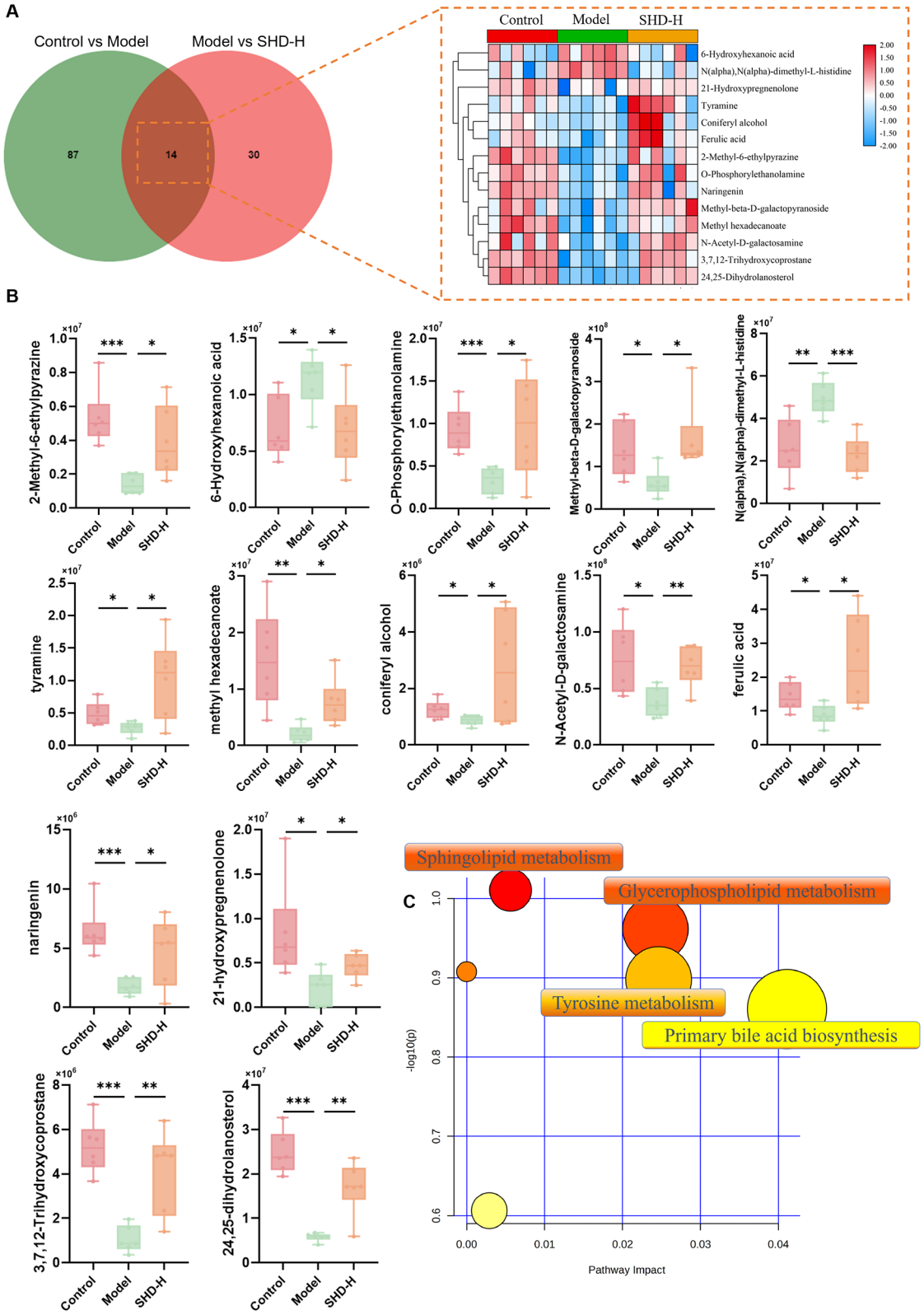

Fig. 6 Differential metabolites and differential metabolic pathways. (**A**) Venn diagram displaying the overlap of differentially expressed metabolites between Control vs. Model and Model vs. SHD-H comparisons. The diagram shows 87 unique metabolites in Control vs. Model, 30 unique metabolites in Model vs. SHD-H, and 14 shared metabolites. Clustered heatmap of 14 differential metabolites on the right. (**B**) levels of 14 metabolites in each group; (**C**) Pathway enrichment analysis of differentially expressed metabolites based on MetaboAnalyst 6.0. Data are presented as mean ± SD, $n = 6$. ***$P < 0.001$, **$P < 0.01$, *$P < 0.05$

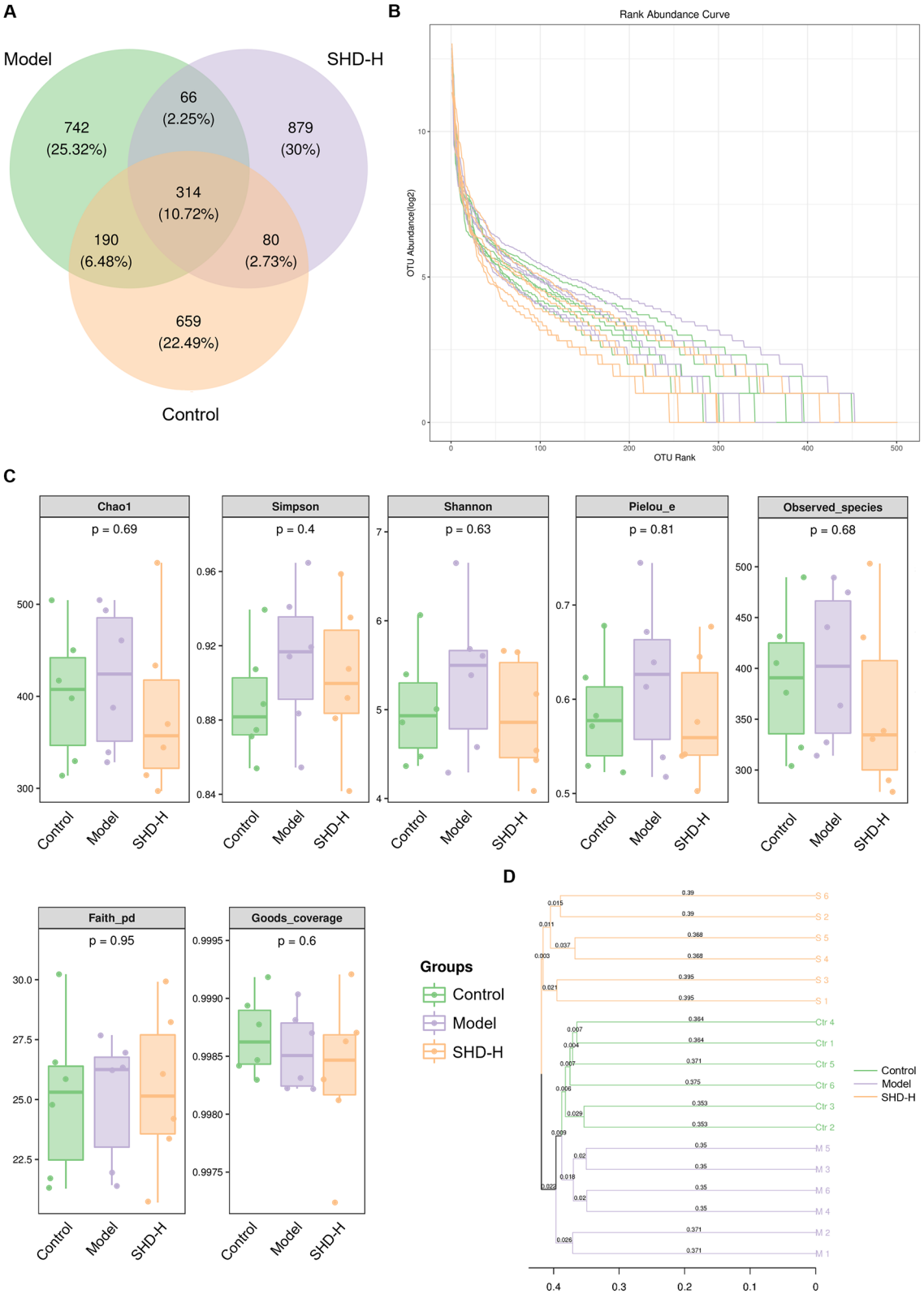

Fig. 7 (See legend on next page.)

(See figure on previous page.)

Fig. 7 Microbiota diversity and composition in fecal samples from Control, Model, and SHD-H groups. (**A**) Venn diagram displaying the overlap of operational taxonomic units (OTUs) among Control, Model, and SHD-H groups. The diagram shows the number and percentage of unique and shared OTUs across the groups, with 314 OTUs shared among all groups. (**B**) Rank abundance curves for the Control, Model, and SHD-H groups. The curves illustrate the richness and evenness of OTUs in each group. (**C**) Box plots of alpha diversity indices, including Chao1, Simpson, Shannon, Pielou_e, Observed_species, Faith_pd, and Goods_coverage, across Control, Model, and SHD-H groups. (**D**) Beta diversity analysis displayed as a bar plot, showing the weighted UniFrac distances among Control, Model, and SHD-H groups. The plot indicates the differences in microbial community composition between the groups, with the y-axis representing different taxa and the x-axis representing the distance

Discussions

SONFH is a condition caused by prolonged or high-dose use of glucocorticoids (GCs), primarily characterized by local blood supply disruption to the femoral head. This disruption leads to the necrosis of bone cells and bone marrow, ultimately resulting in structural damage to the femoral head. Previous study has indicated that GCs can reduce bone density and are associated with trabecular abnormalities and the replacement of bone with necrotic tissue that lacks mechanical strength, severely impacting bone remodeling [22]. In the early stages of SONFH, histological changes in the femoral head may not be significant. However, with the accumulation of mechanical stress and metabolic disturbances, the femoral head may eventually collapse. Thus, early intervention in SONFH is crucial for preventing disease progression. Recently, TCM has garnered significant attention, with numerous clinical trials demonstrating that integrative TCM treatments can enhance efficacy, reduce adverse effects, and slow the progression of ONFH, thereby improving patients' quality of life [23]. Despite the clinical efficacy of SHD, a classical TCM formula, its underlying mechanisms remain unclear. Therefore, our study utilizes network pharmacology, metabolomics, and gut microbiota analyses to systematically elucidate the metabolic and gut microbial profiles of SHD-treated SONFH rats. Additionally, preliminary investigations into the pharmacodynamic mechanisms of SHD in treating SONFH were conducted through in vivo experiments.

In this study, we initially established a rat model of SONFH using a combination of LPS and MPS. Micro-CT, H&E, and Safranin-O-Fast Green staining confirmed that SHD effectively protects against trabecular bone loss in SONFH rats, aligning with previous in vivo findings [24]. It is well-documented that glucocorticoid-induced disruption of osteoblast formation severely impacts bone quality, making it a crucial target for ONFH treatment [25]. To delve deeper, immunohistochemical analysis was performed, revealing that SHD significantly increased the expression levels of osteogenic markers RUNX2, OCN, and COL-I. These results indicate that SHD ameliorates SONFH by enhancing osteogenesis. Furthermore, to elucidate the underlying mechanisms of SHD against SONFH, we utilized UHPLC-Q-Exactive Orbitrap MS in conjunction with network pharmacology. This approach identified several key active components in SHD, including Neocnidilide, Glabridin, Medicarpin, and Licochalcone B. KEGG pathway enrichment analysis further revealed multiple significant signaling pathways, such as Metabolic pathways, MAPK pathways, HIF-1 pathways, and TNF signaling pathways. Among these, Metabolic pathways emerged as particularly significant, underscoring their clinical relevance in therapeutic action of SHD against SONFH.

To further clarify the critical role of Metabolic pathways in SHD intervention for SONFH, we conducted a fecal metabolomics study on the Control, Model, and SHD-H groups using GC-TOF/MS. The results revealed that 14 differential metabolites changed after the SONFH model was established and were reversed following SHD treatment. These metabolites included flavonoids, phenolic metabolites, fatty acids, carbohydrates, cholesterol derivatives, amino acid derivatives, and steroid metabolites. Among them, Ferulic Acid and Naringenin are closely associated with anti-inflammatory and antioxidant activities. Studies have shown that both Ferulic Acid and Naringenin can promote osteogenic differentiation of bone marrow mesenchymal stem cells and prevent bone loss [26, 27]. O-Phosphorylethanolamine, a precursor of phosphatidylethanolamine, plays a crucial role in bone matrix mineralization, potentially affecting bone formation and remodeling [28]. 6-Hydroxyhexanoic acid, a medium-chain fatty acid metabolite, is involved in fatty acid metabolism and energy balance, with research linking fatty acids closely to bone metabolism and related bone diseases [29]. 21-Hydroxyprogesterone serves as a crucial precursor in the synthesis of cortisol, which, as a member of the glucocorticoid class of hormones, exerts a significant influence on skeletal health. Scientific literature has demonstrated excessive glucocorticoids can induce apoptosis in osteocytes and osteoblasts, reduce bone matrix synthesis, and accelerate the progression of femoral head necrosis by affecting bone remodeling [30]. The remaining differential metabolites have not yet been reported in the context of bone metabolism or femoral head necrosis, presenting potential new directions for future research. Metabolic pathway analysis of the 14 differential metabolites using MetaboAnalyst revealed significant enrichment in sphingolipid metabolism, glycerophospholipid metabolism, tyrosine metabolism, and primary bile acid biosynthesis. Sphingolipid and glycerophospholipid metabolism are closely related to lipid metabolism. Disruptions in lipid metabolism have been identified as crucial metabolic features of ONFH

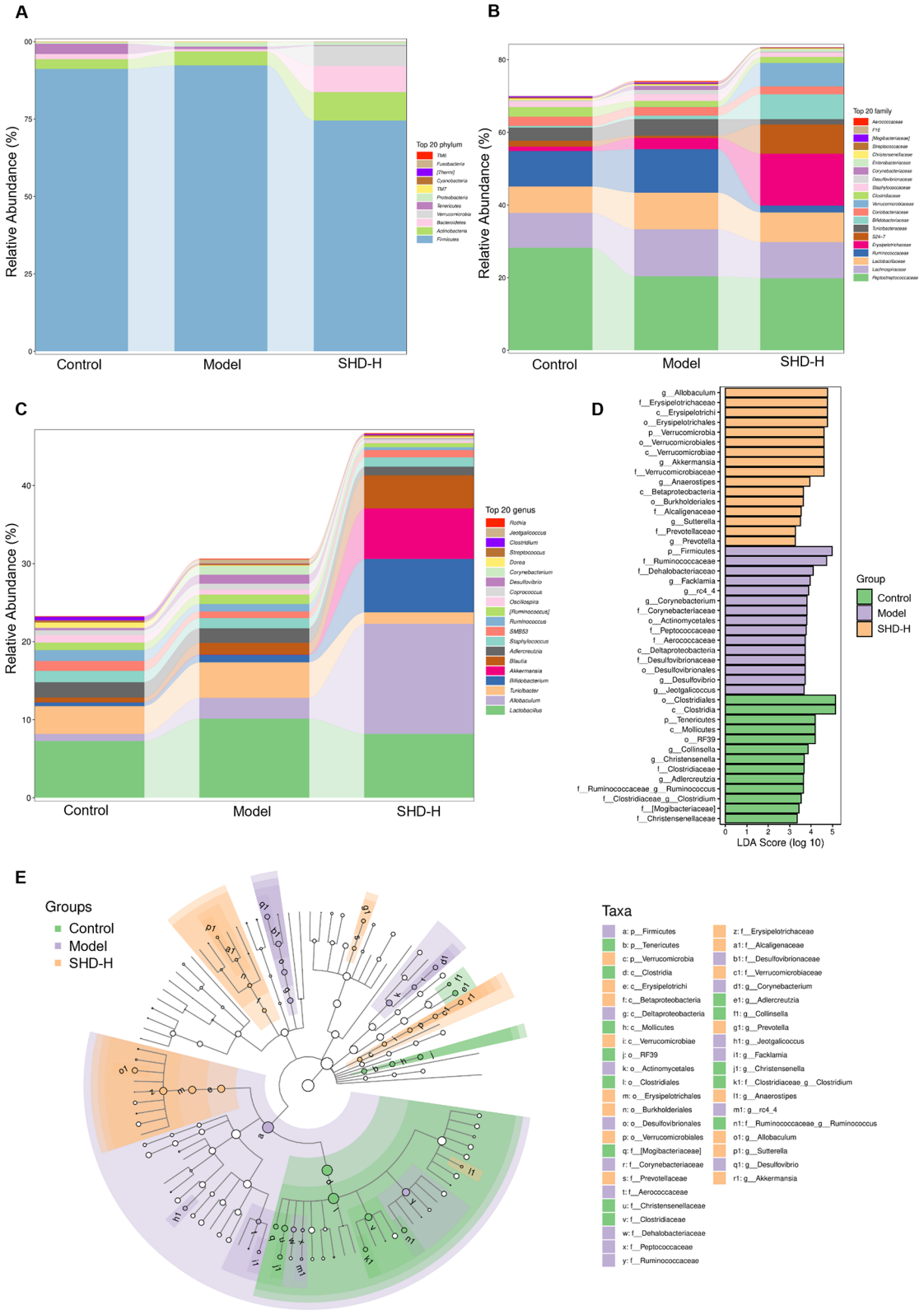

Fig. 8 Taxonomic composition and differential abundance analysis of gut microbiota in different groups. (**A-C**) Stacked bar charts showing the relative abundance of the top 20 bacterial taxa at different taxonomic levels in fecal samples from Control, Model, and SHD-H groups: Phylum level (**A**), Family level (**B**), Genus level (**C**). (**D**) Linear discriminant analysis (LDA) effect size (LEfSe) analysis identifying the most differentially abundant taxa among the Control, Model, and SHD-H groups. (**E**) Cladogram generated by LEfSe analysis showing the phylogenetic distribution of significantly different taxa among Control, Model, and SHD-H groups

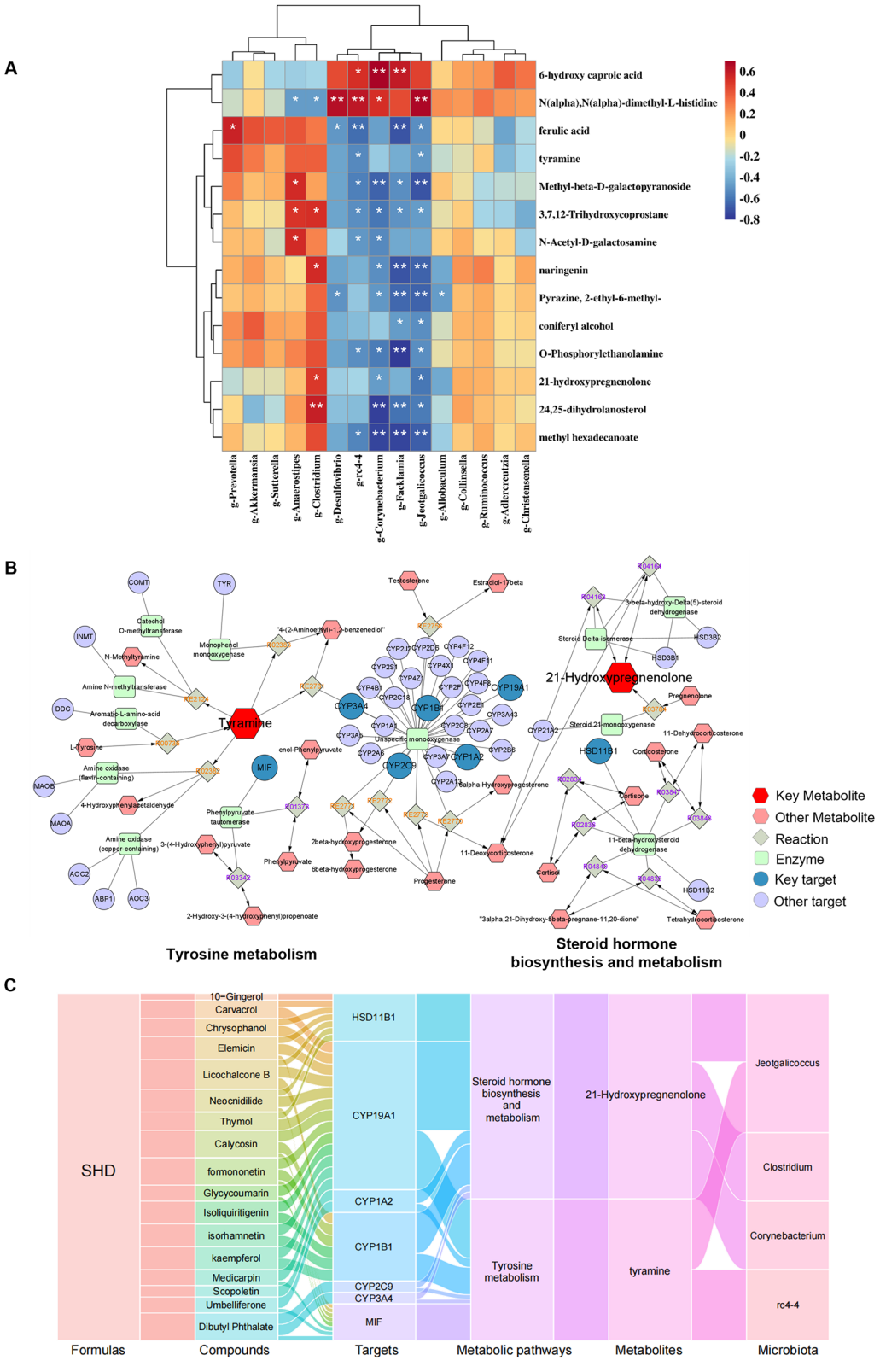

Fig. 9 (See legend on next page.)

(See figure on previous page.)

Fig. 9 Integrated analysis involving gut microbiota, metabolomics and network pharmacology. (**A**) Heat map of the association between differential gut microbiota and differential metabolites. Significant differences are indicated by $*P < 0.05$ and $**P < 0.01$. (**B**) The Metabolite-Reaction-Enzyme-Target network illustrating the interactions between metabolites, targets, and enzymes via MetScape plugin. It identified 2 pivotal metabolic pathways (tyrosine metabolism, steroid hormone biosynthesis, and metabolism). (**C**) Sankey diagram depicting Herbs-Targets-Pathways-Metabolites-Microbiota interactions. Herbs section, only herbs containing key targets were shown; Metabolic pathways section, only metabolic pathways enriched for key targets and differential metabolites; Metabolites section, only the set of metabolites captured by metabolic pathways; Microbiota section, only the set of genera with differential metabolites correlations greater than 0.5

[31, 32]. Thus, SHD may improve SONFH by modulating lipid metabolism through these pathways. Primary bile acid biosynthesis, a critical biochemical process in the liver, converts cholesterol to bile acids. Research has found that bile acids can activate FXR, upregulate Runx2, and enhance the extracellular signal-regulated kinase (ERK) and β-catenin signaling pathways, significantly promoting osteoblast differentiation [33]. Additionally, tyrosine metabolism involves key components such as tyrosine kinases and their downstream signaling molecules, which play essential roles in bone metabolism. A recent study indicates that tyrosine kinase Src can influence bone metabolism by regulating osteoblast-mediated bone formation and osteoclast-mediated bone resorption [34]. Therefore, it is plausible that SHD may regulate bone metabolism through multiple metabolic pathways, thereby impacting SONFH.

Metabolomics analyses have revealed that SHD influences fecal metabolites in SONFH rats, with gut microbiota playing a pivotal role in host metabolic pathways through their metabolites. The gut microbiota, a complex and dynamic community of approximately 100 trillion microorganisms—including bacteria, viruses, fungi, and protozoa—is now recognized as an essential organ for human health [35, 36]. Research underscores that gut microbiota can regulate bone metabolism by modulating the immune system, nutrient absorption, and gut permeability [37, 38]. In our study, 16S rRNA sequencing was performed on fecal samples from Control, Model, and SHD-H groups, followed by LEfSe analysis to identify significantly different bacterial species. Post-SONFH model induction, notable changes were observed in species such as *Aerococcaceae*, *Ruminococcaceae*, *Corynebacteriaceae*, *Desulfovibrionales*, and *Facklamia*, suggesting their close association with SONFH. Particularly, *Ruminococcus*, a genus within the *Ruminococcaceae* family, is prominent in gut microbiota and considered a potential probiotic. Research indicates that *Ruminococcus* abundance is higher in healthy individuals compared to those with osteoporosis [39, 40]. Additionally, oral strontium ranelate has been shown to significantly increase *Ruminococcus* abundance in OVX rats, highlighting its importance in bone metabolism [41]. Similarly, the *Desulfovibrionales* order, including sulfate-reducing bacteria, significantly impacts gut metabolism by producing hydrogen sulfide (H_2S), which plays a crucial role in bone metabolism. H_2S influences the protein profile of M_2 macrophage exosomes, promoting osteogenic differentiation of mesenchymal stem cells (MSCs) through moesin-mediated endocytosis and activation of the β-catenin signaling pathway [42]. Although other identified species lack direct or indirect links to femoral head necrosis, they might influence bone health through immune modulation or metabolite production, necessitating further study. SHD treatment resulted in significant alterations in gut microbiota composition, notably in *Verrucomicrobia*, *Verrucomicrobiaceae*, *Allobaculum*, *Erysipelotrichales*, and *Burkholderiales*. Previous studies have shown that members of *Verrucomicrobia*, especially *Akkermansia muciniphila*, degrade intestinal mucin and produce short-chain fatty acids (SCFAs) [43]. SCFAs are known to stimulate bone formation and inhibit bone resorption by regulating Treg cell secretion [44, 45], thereby improving bone metabolism in the necrotic area of the femoral head. *Verrucomicrobiaceae*, within *Verrucomicrobia*, likely exhibit similar functions. Additionally, SCFA levels are positively correlated with the abundance of *Allobaculum* [46]. Wang et al. found significant correlations between *Erysipelotrichales* and serum levels of bone Gla-protein (BGP), receptor activator of nuclear factor-kappa B (RANK), receptor activator of nuclear factor-kappa B ligand (RANKL), osteoprotegerin (OPG), and tartrate-resistant acid phosphatase (TRACP) [47]. These findings suggest that *Verrucomicrobia*, *Verrucomicrobiaceae*, *Allobaculum*, *Erysipelotrichales*, and *Burkholderiales* are key microbial communities influenced by SHD. SHD likely improves SONFH by modulating these gut microbiota, thereby regulating bone metabolism.

In our study, we integrated data from network pharmacology and metabolomics to construct a comprehensive "metabolite-reaction-enzyme-target" network. This network revealed 2 key differential metabolites (tyramine, 21-hydroxypregnenolone), 7 critical targets (CYP19A1, CYP1A2, CYP1B1, CYP2C9, CYP3A4, MIF, HSD11B1), and 2 pivotal metabolic pathways (tyrosine metabolism, steroid hormone biosynthesis, and metabolism), which are central to the therapeutic effects of SHD on SONFH. Five of the seven key targets are members of the cytochrome P450 enzyme family, essential for the synthesis and metabolism of endogenous substances such as hormones, fatty acids, and cholesterol [48]. Additionally, MIF (macrophage migration inhibitory factor) emerges as a multifunctional pro-inflammatory mediator that regulates immune responses and is implicated in various

pathological and physiological states [49]. Research by Zheng et al. has shown that MIF can inhibit osteoblast-mediated mineralization and bone nodule formation in vitro [50]. Conversely, MIF inhibitors promote the expression of osteogenic markers like RUNX2, OCN, and COL-I by inhibiting the NF-κB signaling pathway [51], suggesting a potential mechanistic parallel with SHD. HSD11B1, another significant target, is involved in glucocorticoid synthesis. Overexpression of HSD11B1 in osteoblasts suppresses osteogenic differentiation and, through activation of the Hippo signaling pathway, can promote osteoclastogenesis, thus contributing to osteoporosis [52–54]. Therefore, it is plausible that HSD11B1 accelerates SONFH progression, making it a crucial target for SHD.

In addition, Spearman correlation analysis based on available microbiome and metabolomics data was conducted. This analysis identified significant correlations between 14 differential metabolites and 15 bacterial genera. In "compound-target-metabolic pathway-metabolite-gut microbiota" network, we highlighted 4 key bacterial genera: *Jeotgalicoccus*, *Clostridium*, *Corynebacterium*, and *rc4-4*. Despite limited direct evidence linking these genera to SONFH, their potential roles warrant attention. It is well-documented that gut microbiota influence distant host organs via circulating molecules, including microbiota-derived or induced metabolites, hormones, and neurotransmitters. Notably, gut microbiota have been shown to impact distal bone remodeling, promoting both bone resorption and formation [55]. Our findings suggest that SHD may modulate these bacterial genera to influence related metabolite levels, thereby regulating bone remodeling and exerting therapeutic effects on SONFH.

Conclusions

This study, integrating in vivo experiments, network pharmacology, metabolomics, and gut microbiota analyses, demonstrated that SHD ameliorates SONFH by reshaping gut microbiota and regulating host metabolism. SHD significantly altered the abundance of microbial taxa, including Verrucomicrobia, Allobaculum, Verrucomicrobiaceae, Erysipelotrichales, and Burkholderiales. Moreover, it reversed the levels of 14 differential metabolites, such as 21-hydroxypregnenolone and tyramine, restoring metabolic balance in pathways like tyrosine metabolism and steroid hormone biosynthesis. This metabolic rebalancing was accompanied by an increase in the expression of osteogenic factors, collectively contributing to the therapeutic efficacy of SHD against SONFH. Our research deepens the understanding of the pharmacodynamic mechanisms of SHD, providing a robust foundation for its clinical application. Notably, this comprehensive approach underscores the potential of SHD as a promising treatment for SONFH, highlighting its capacity to modulate key biological pathways and gut microbiota involved in bone health.

Supplementary Information

The online version contains supplementary material available at https://doi.org/10.1186/s13018-025-05619-0.

Supplementary Material 1

Author contributions

Q.W. and J.Z. conceived and supervised the study. G.D. and K.Z. designed the experiments. K.Z., W.L., Y.P., X.W. and Z.W. performed the experiments and acquired the data. K.Z., W.L. and Y.P. analyzed the data. K.Z. and W.L. drafted the manuscript. J.Z., G.D. and Q.W. critically revised the manuscript. All authors reviewed the manuscript.

Funding

This work was supported by the National Natural Science Foundation of China (NO. 82172443) and the Key Project (2019YYZ10) of Integrated Traditional Chinese and Western Medicine at Yueyang Hospital of Integrated Traditional Chinese and Western Medicine affiliated with Shanghai University of Traditional Chinese Medicine.

Data availability

No datasets were generated or analysed during the current study.

Declarations

Competing interests

The authors declare no competing interests.

Author details

[1]Yueyang Hospital of Integrated Traditional Chinese and Western Medicine, Shanghai University of Traditional Chinese Medicine, Shanghai 200437, P.R. China
[2]Shanghai General Hospital, Shanghai Jiao Tong University School of Medicine, Shanghai 201620, P.R. China

Received: 26 December 2024 / Accepted: 17 February 2025
Published online: 26 February 2025

References

1. Hua K, Yang X, Feng J, Wang F, Yang L, Zhang H, et al. The efficacy and safety of core decompression for the treatment of femoral head necrosis: a systematic review and meta-analysis. J Orthop Surg Res. 2019;14:306.
2. Zhang F, Wei L, Wang L, Wang T, Xie Z, Luo H, et al. FAR591 promotes the pathogenesis and progression of SONFH by regulating Fos expression to mediate the apoptosis of bone microvascular endothelial cells. Bone Res. 2023;11:27.
3. Li T, Zhang Y, Wang R, Xue Z, Li S, Cao Y, et al. Discovery and validation an eight-biomarker serum gene signature for the diagnosis of steroid-induced osteonecrosis of the femoral head. Bone. 2019;122:199–208.
4. Quaranta M, Miranda L, Oliva F, Aletto C, Maffulli N. Osteotomies for avascular necrosis of the femoral head. Br Med Bull. 2021;137:98–111.
5. Sadile F, Bernasconi A, Russo S, Maffulli N. Core decompression versus other joint preserving treatments for osteonecrosis of the femoral head: a meta-analysis. Br Med Bull. 2016;118:33–49.
6. Migliorini F, La Padula G, Oliva F, Torsiello E, Hildebrand F, Maffulli N. Operative management of avascular necrosis of the femoral head in skeletally immature patients: A systematic review. Life. 2022;12:179.
7. Migliorini F, Maffulli N, Baroncini A, Eschweiler J, Tingart M, Betsch M. Prognostic factors in the management of osteonecrosis of the femoral head: A systematic review. Surgeon. 2023;21:85–98.

8. Migliorini F, Maffulli N, Eschweiler J, Tingart M, Baroncini A. Core decompression isolated or combined with bone marrow-derived cell therapies for femoral head osteonecrosis. Expert Opin Biol Ther. 2021;21:423–30.
9. Li S, Liu Y, Zhou G, Zhang W, Wei S, He J, et al. Pre-collapse femoral head necrosis treated by hip abduction: a computational Biomechanical analysis. Health Inf Sci Syst. 2022;10:8.
10. Li H, Zhang Y, Hao Y, Xu P, Wang X, Zhu B, et al. Proanthocyanidins inhibit osteoblast apoptosis via the PI3K/AKT/Bcl-xL pathway in the treatment of Steroid-Induced osteonecrosis of the femoral head in rats. Nutrients. 2023;15:1936.
11. Liu C, Wang C, Liu Y, Huang J, Xu W, Li J, et al. Selenium nanoparticles/carboxymethyl Chitosan/alginate antioxidant hydrogel for treating steroid-induced osteonecrosis of the femoral head. Int J Pharm. 2024;653:123929.
12. Chen J, Ye C, Yang Z, Zhang C, Li P, Xu B, et al. Erchen Decoction to reduce oxidative stress in dyslipidemia phlegm-dampness retention syndrome mice: in vivo mechanism revealed by metabolomics (liquid chromatography-mass spectrometry). Phytomedicine. 2023;115:154808.
13. Lu X, Li J, Zhou B, Lu X, Li W, Ouyang J. Taohong Siwu Decoction enhances human bone marrow mesenchymal stem cells proliferation, migration and osteogenic differentiation via VEGF-FAK signaling in vitro. J Ethnopharmacol. 2023;307:116203.
14. Shi Y, Wang S, Deng D, Wang Y. Taohong Siwu Decoction: a classical Chinese prescription for treatment of orthopedic diseases. Chin J Nat Med. 2024;22:711–23.
15. Liu H, Cai Z, Chen M, Shen J, Xia T, Wei A. Clinical effects of Shuanghe Decoction combined with minimally invasive hip-preserving surgery on patients with non-traumatic osteonecrosis of the femorahead in peri-collapse stage. Chin J Inf Tradit Chin Med. 2023;30(02):135–40. https://doi.org/10.19879/j.cnki.1005-5304.202204561). https://link.cnki.net/doi/.
16. Hou W, Du B, Liu X, Chen H, Chen Y, Gao F. Research progress of common compound of femoral head necrosis. F Tradit Chin Med. 2022;37(02):71–5. https://doi.org/10.13913/j.cnki.41-1110/r.2022.02.001). https://link.cnki.net/doi/.
17. Niu B, Zhang H, Li C, Yan F, Song Y, Hai G, et al. Network Pharmacology study on the active components of pterocypsela Elata and the mechanism of their effect against cerebral ischemia. Drug Des Dev Ther. 2019;13:3009–19.
18. Huang Q, Liu R, Liu J, Huang Q, Liu S, Jiang Y. Integrated network Pharmacology analysis and experimental validation to reveal the mechanism of Anti-Insulin resistance effects of Moringa oleifera seeds. Drug Des Dev Ther. 2020;14:4069–84.
19. Wang C, Jiang S, Zhang S, Ouyang Z, Wang G, Wang F. Research progress of metabolomics in asthma. Metabolites. 2021;11:567.
20. Gao Y, You Y, Zhang P, Yu Y, Xu Z, Wei H, et al. Cortistatin prevents glucocorticoid-associated osteonecrosis of the femoral head via the GHSR1a/Akt pathway. Commun Biol. 2024;7:132.
21. Yuan S, Zhang C, Wang B. Neohesperidin promotes the proliferation and osteogenic differentiation of BMSCs via BMP2-Wnt/β-catenin pathway. Cell Cycle. 2022;21:187–201.
22. Walsh LJ, Lewis SA, Wong CA, Cooper S, Oborne J, Cawte SA, et al. The impact of oral corticosteroid use on bone mineral density and vertebral fracture. Am J Respir Crit Care Med. 2002;166:691–5.
23. Ouyang W, Meng Y, Guo G, Zhao C, Zhou X. Efficacy and safety of traditional Chinese medicine in the treatment of osteonecrosis of the femoral head. J Orthop Surg Res. 2023;18:600.
24. Li Z, Zhou L, Duan Z, Li X, Qi Z. Study on effect of Shuanghe Decoction on biomechanics of steroid-induced avascular necrosis of femoral head. J Liaoning Tradit Chin Med. 2017;44(01):163–6.
25. Zhou M, Xi J, Cheng Y, Sun D, Shu P, Chi S, et al. Reprogrammed mesenchymal stem cells derived from iPSCs promote bone repair in steroid-associated osteonecrosis of the femoral head. Stem Cell Res Ther. 2021;12:175.
26. Du K, Li Z, Fang X, Cao T, Xu Y. Ferulic acid promotes osteogenesis of bone marrow-derived mesenchymal stem cells by inhibiting microRNA-340 to induce β-catenin expression through hypoxia. Eur J Cell Biol. 2017;96:496–503.
27. Wang Y, Bai S, Cheng Q, Zeng Y, Xu X, Guan G. Naringenin promotes SDF-1/CXCR4 signaling pathway in BMSCs osteogenic differentiation. Folia Histochem Cytobiol. 2021;59:66–73.
28. Sekaran S, Vimalraj S, Thangavelu L. The physiological and pathological role of tissue nonspecific alkaline phosphatase beyond mineralization. Biomolecules. 2021;11:1564.
29. Bao M, Zhang K, Wei Y, Hua W, Gao Y, Li X, et al. Therapeutic potentials and modulatory mechanisms of fatty acids in bone. Cell Prolif. 2020;53:e12735.
30. Yuan N, Zhang W, Yang W, Ji W, Li J. Exosomes derived from M2 macrophages prevent steroid-induced osteonecrosis of the femoral head by modulating inflammation, promoting bone formation and inhibiting bone resorption. J Orthop Surg Res. 2024;19:243.
31. Guo M, Zhang J. Metabolomic analysis of bone-derived exosomes in osteonecrosis of the femoral head based on UPLC-MS/MS. Metabolomics. 2023;19:34.
32. Zhu W, Chen T, Ding S, Yang G, Xu Z, Xu K, et al. Metabolomic study of the bone trabecula of osteonecrosis femoral head patients based on UPLC–MS/MS. Metabolomics. 2016;12:48.
33. Cho SW, An JH, Park H, Yang J, Choi HJ, Kim SW, et al. Positive regulation of osteogenesis by bile acid through FXR. J Bone Min Res. 2013;28:2109–21.
34. Matsubara T, Yasuda K, Mizuta K, Kawaue H, Kokabu S. Tyrosine kinase Src is a regulatory factor of bone homeostasis. Int J Mol Sci. 2022;23:5508.
35. Oliphant K, Allen-Vercoe E. Macronutrient metabolism by the human gut microbiome: major fermentation by-products and their impact on host health. Microbiome. 2019;7:91.
36. Valdes AM, Walter J, Segal E, Spector TD. Role of the gut microbiota in nutrition and health. BMJ. 2018;361:k2179.
37. Chevalier C, Kieser S, Çolakoğlu M, Hadadi N, Brun J, Rigo D, et al. Warmth prevents bone loss through the gut microbiota. Cell Metab. 2020;32:575–90.
38. de Sire A, de Sire R, Curci C, Castiglione F, Wahli W. Role of dietary supplements and probiotics in modulating microbiota and bone health: the Gut-Bone Axis. Cells. 2022;11:743.
39. Ma S, Qin J, Hao Y, Fu L. Association of gut microbiota composition and function with an aged rat model of senile osteoporosis using 16S rRNA and metagenomic sequencing analysis. Aging. 2020;12:10795–808.
40. Xu Z, Xie Z, Sun J, Huang S, Chen Y, Li C, et al. Gut Microbiome reveals specific dysbiosis in primary osteoporosis. Front Cell Infect Microbiol. 2020;10:160.
41. Xiao X, Cui Y, Lu H, Wang J, Yang J, Liu L, et al. Strontium Ranelate enriched Ruminococcus albus in the gut Microbiome of Sprague-Dawley rats with postmenopausal osteoporosis. BMC Microbiol. 2023;23:365.
42. Zhou Y, Han C, Zhu Z, Chen P, Wang Y, Lin S, et al. M_2 exosomes modified by hydrogen sulfide promoted bone regeneration by Moesin mediated endocytosis. Bioact Mater. 2024;31:192–205.
43. Lordan C, Thapa D, Ross RP, Cotter PD. Potential for enriching next-generation health-promoting gut bacteria through prebiotics and other dietary components. Gut Microbes. 2020;11:1–20.
44. McHugh J. Wnt signalling in the gut microbiota-bone axis. Nat Rev Rheumatol. 2019;15:4.
45. Zaiss MM, Jones RM, Schett G, Pacifici R. The gut-bone axis: how bacterial metabolites bridge the distance. J Clin Invest. 2019;129:3018–28.
46. Wang D, Wang L, Han L, Wang B, Shi R, Ye J, et al. Leucine-Restricted Diet Ameliorates Obesity-Linked Cognitive Deficits: Involvement of the Microbiota-Gut-Brain Axis. J Agric Food Chem. 2023;71:9404–18.
47. Wang S, Wang S, Wang X, Xu Y, Zhang X, Han Y, et al. Effects of Icariin on Modulating Gut Microbiota and Regulating Metabolite Alterations to Prevent Bone Loss in Ovariectomized Rat Model. Front Endocrinol. 2022;13:874849.
48. Machalz D, Pach S, Bermudez M, Bureik M, Wolber G. Structural insights into understudied human cytochrome P450 enzymes. Drug Discov Today. 2021;26:2456–64.
49. Jin K, Zheng L, Ye L, Xie Z, Gao J, Lou C, et al. Chicago sky blue 6B (CSB6B), an allosteric inhibitor of macrophage migration inhibitory factor (MIF), suppresses osteoclastogenesis and promotes osteogenesis through the inhibition of the NF-κB signaling pathway. Biochem Pharmacol. 2021;192:114734.
50. Zheng L, Gao J, Jin K, Chen Z, Yu W, Zhu K, et al. Macrophage migration inhibitory factor (MIF) inhibitor 4-IPP suppresses osteoclast formation and promotes osteoblast differentiation through the inhibition of the NF-κB signaling pathway. Faseb J. 2019;33:7667–83.
51. Shi X, Wu Y, Ni H, Li M, Qi B, Xu Y. Macrophage migration inhibitory factor (MIF) inhibitor iSO-1 promotes staphylococcal protein A-induced osteogenic differentiation by inhibiting NF-κB signaling pathway. Int Immunopharmacol. 2023;115:109600.
52. Blaschke M, Koepp R, Streit F, Beismann J, Manthey G, Seitz M, et al. The rise in expression and activity of 11β-HSD1 in human mesenchymal progenitor cells induces adipogenesis through increased local cortisol synthesis. J Steroid Biochem Mol Biol. 2021;210:105850.
53. Li H, Hu S, Wu R, Zhou H, Zhang K, Li K, et al. 11β-Hydroxysteroid dehydrogenase type 1 facilitates osteoporosis by turning on osteoclastogenesis through Hippo signaling. Int J Biol Sci. 2023;19:3628–39.

54. Park JS, Bae SJ, Choi S, Son YH, Park SB, Rhee SD, et al. A novel 11β-HSD1 inhibitor improves diabesity and osteoblast differentiation. J Mol Endocrinol. 2014;52:191–202.
55. Yan J, Takakura A, Zandi-Nejad K, Charles JF. Mechanisms of gut microbiota-mediated bone remodeling. Gut Microbes. 2018;9:84–92.

Publisher's note